Featuring work from the group of Professor Liang Dong at the Iowa State University.

Title: Plant chip for high-throughput phenotyping of Arabidopsis

A vertical plant chip is developed for high-throughput and large-scale phenotyping of *Arabidopsis thaliana* plants. Multiple seeds can be germinated and grown hydroponically up to four weeks in the chip. The vertical arrangement of the chip makes it convenient to continuously monitor plant–pathogen interactions at different developmental stages, and phenotypic changes in plants at the whole organismal level, including seed germination and root and shoot growth, as well as at the cellular level.

As featured in:

See Huawei Jiang *et al.*, *Lab Chip*, 2014, **14**, 1281.

ROYAL SOCIETY OF CHEMISTRY

www.rsc.org/loc

Registered charity number: 207890

Lab on a Chip

PAPER

View Article Online
View Journal | View Issue

Cite this: *Lab Chip*, 2014, **14**, 1281

Plant chip for high-throughput phenotyping of *Arabidopsis*†

Huawei Jiang,[a] Zhen Xu,[a] Maneesha R Aluru*[b] and Liang Dong*[a]

We report on the development of a vertical and transparent microfluidic chip for high-throughput phenotyping of *Arabidopsis thaliana* plants. Multiple *Arabidopsis* seeds can be germinated and grown hydroponically over more than two weeks in the chip, thus enabling large-scale and quantitative monitoring of plant phenotypes. The novel vertical arrangement of this microfluidic device not only allows for normal gravitropic growth of the plants but also, more importantly, makes it convenient to continuously monitor phenotypic changes in plants at the whole organismal level, including seed germination and root and shoot growth (hypocotyls, cotyledons, and leaves), as well as at the cellular level. We also developed a hydrodynamic trapping method to automatically place single seeds into seed holding sites of the device and to avoid potential damage to seeds that might occur during manual loading. We demonstrated general utility of this microfluidic device by showing clear visible phenotypes of the *immutans* mutant of *Arabidopsis*, and we also showed changes occurring during plant–pathogen interactions at different developmental stages. *Arabidopsis* plants grown in the device maintained normal morphological and physiological behaviour, and distinct phenotypic variations consistent with *a priori* data were observed *via* high-resolution images taken in real time. Moreover, the timeline for different developmental stages for plants grown in this device was highly comparable to growth using a conventional agar plate method. This prototype plant chip technology is expected to lead to the establishment of a powerful experimental and cost-effective framework for high-throughput and precise plant phenotyping.

Received 29th November 2013,
Accepted 3rd January 2014

DOI: 10.1039/c3lc51326b

www.rsc.org/loc

Introduction

The recent completion of the genome sequencing projects, along with advances in high-throughput technologies (*e.g.*, microarrays, next generation sequencing), have made it possible for a high-throughput "systems approach" to acquire a great wealth of information about the genotype, *i.e.*, the genetic makeup of an organism.[1–7] Much of the existing instrumentation and software have also been built with the key goal of identifying and analysing various biomolecules (*e.g.*, DNA, RNA, metabolites). But information about the genotype is only useful in so far as it allows us to make predictions about the phenotype, *i.e.*, the observable traits and characteristics of an organism. Phenomics is an emerging area of science that links observations on genotypes with phenotypes.[8,9] However, characterization of the complete plant phenome poses a difficult challenge, as even plants with smaller genomes such as *Arabidopsis thaliana* contain tens of thousands of genes.[10–12]

Previous plant phenotype analyses relied on culturing seeds and growing plants in soil pots and agarose plates using culture facilities (*e.g.*, greenhouse, growth chamber) under controlled environments, and on using imaging technology to measure plant characteristics and phenotypic changes.[13–19] Multi-well plates have also been utilized for chemical screening of a large number of seedling roots.[20,21] However, there are several concerns worth noting. First, screening of plant phenotypes using traditional greenhouses and growth chambers is costly and the number of experiments is limited. Flexibility and accuracy of changing plant growth environments are also relatively low. Second, due to the use of soil pots and agarose plates, a relatively large amount of chemicals and biological species is needed. Third, spatial resolution of morphological measurements for seed, root, and shoot phenotypes is often on the millimetre scale as soil pots and agarose plates are not optically transparent. Real-time observation of cellular behaviours (*e.g.*, cell division, elongation, host–pathogen interactions) is also not easy. As a result, low temporal resolution may lead to missing information about progressive and subtle changes in phenotypes during plant growth. Therefore, while progress has been

[a] *Department of Electrical and Computer Engineering, Iowa State University, Ames, IA 50011, USA. E-mail: ldong@iastate.edu; Fax: +1 515 294 8432; Tel: +1 515 294 0388*
[b] *School of Biology, Georgia Institute of Technology, Atlanta, GA 30332, USA. E-mail: maneesha.aluru@biology.gatech.edu*

† Electronic supplementary information (ESI) available: A video shows microfluidic trapping of *Arabidopsis* seeds within a vertical microfluidic plant phenotyping device. See DOI: 10.1039/c3lc51326b

made in this area, the traditional plant phenotyping approaches suffer from expense, labour, and time involved in large-scale phenotypic analyses (especially under varying environmental conditions), low spatial and temporal resolution, low throughput for obtaining phenotype information, and frequent manual intervention during growth and imaging.[22–24]

Microfluidic technology provides a powerful and flexible platform to interrogate cellular and multicellular organisms. The general advantages of microfluidics-based bioassays include high throughput and improved data statistic due to parallel processing, reduction of agent consumption, fast reaction, and avoidance of contamination. Prior developments in microfluidic devices have greatly advanced high-throughput analyses of model organisms, such as *Drosophila melanogaster* and *Caenorhabditis elegans*.[25–30] But microfluidic technology is still relatively underdeveloped and underutilized for applications in plant sciences, an area with huge social and economic impact.

Recently, *Arabidopsis* root development and *Camellia* pollen tube growth have been studied using microfluidic devices.[31–36] A RootChip was developed for high-throughput plant gene expression analysis,[32] where *Arabidopsis* seeds germinated and grew initially in conventional pipettes for several days, and then, transferred into the chip for root gene expression studies. More recently, a RootArray was reported, where multiple *Arabidopsis thaliana* seedlings grew in the chip and their roots were imaged using confocal laser scanning microscopy over several days.[35] Our group also developed a microfluidic device for in-chip seed germination and seedling growth at different growth temperatures over several days, thus expanding the utility of microfluidic technology for manipulating plant environmental conditions.[33] Although these approaches have advanced the use of microfluidics in plant sciences, phenotypic measurements with these devices were restricted *only* to plant roots,[32–36] and quantitative measurements of other organ phenotypes (*e.g.*, seed germination, hypocotyl, cotyledon, leaf growth) were not feasible. Therefore, the existing microfluidic devices are of limited use for characterization of the complete plant phenome.

Here, we report on the development of a novel microfluidic device for high-throughput phenotyping of *Arabidopsis* plants. Unlike the previous microfluidic devices where the plant roots were grown horizontally in microchannels, specimen transfer was sometimes required after a certain period of growth, and phenotypic measurement was allowed only for root systems over a relatively short growth time, the present device consists of a transparent and vertical microfluidic chip where multiple *Arabidopsis* seeds can be germinated and grown vertically in the chip, not only allowing for normal gravitropic growth of the plants but also, more importantly, making it convenient for continuous and non-invasive monitoring of phenotypic changes of different plant organs, including both root and shoot systems, over various plant developmental stages. Also, in the present device, *Arabidopsis* plants can grow over a longer growth period than the existing devices (*i.e.*, more than two weeks *vs.* several days).

Methods and experimental section

Overall design of device

Fig. 1a shows the schematic of the present microfluidic plant chip. The device allows multiple plants to simultaneously grow in vertical direction in multiple growth regions. Each growth region includes a funnel-shaped seed holding site on the top and a tapered expanding microchannel on the bottom. The seeds are germinated inside the seed holding sites. The plant roots grow downward into the tapered channel. The main channel above the seed holding sites allows sufficient space for the plant shoots to grow upward (Fig. 1a). To accommodate phenotyping of different plant species growing at different stages of interest, the number of the seed holding sites and the structure and geometry of the root and shoot growth regions can be flexibly changed during device design and fabrication. In the device presented here, 26 *Arabidopsis* plants are distributed on two connecting floors. To hold *Arabidopsis* seeds and provide enough room for seed germination, the lower and upper openings of the funnel are designed to be 350 μm and 725 μm wide, respectively. The root and shoot growth regions are designed to be 10 mm and 1.8 mm tall, respectively. All of the channels of the device are 400 μm deep. In the case that the main channel is closed (Fig. 1b), the plants can grow within the device for about eleven days, during which seed germination and emergence and growth of plant root, hypocotyl, cotyledon, and the first two true leaves can be clearly imaged. By opening up the main channel of the device, the plants can grow over more than two weeks and the plant

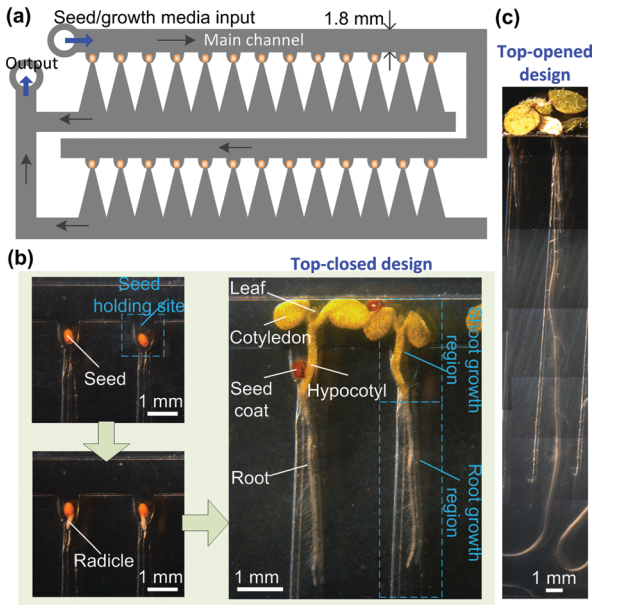

Fig. 1 (a) Schematic of the plant chip for high-throughput plant phenotyping. (b) In-chip seed germination and plant growth. Major plant organs and device structures are labelled and highlighted. In this top-closed design, the main channel is closed during the growth of the plants. (c) A top-opened design for plant phenotyping over a longer growth period. The top part of the main channel is cut off. The shoot system of the plants is grown outside of the top-opened device.

phenotypes through later growth stages can be observed and recorded (Fig. 1c). This transparent device, in conjunction with a conventional microscopic imaging system, can facilitate easy and high-quality observation of plant phenotypes at the whole organismal as well as at the cellular level.

Design for hydrodynamic trapping of seeds

Generally, individual *Arabidopsis* seeds are handled by using sterilized tools such as toothpicks or forceps. Due to their small size, it would be difficult to manually pick and load seeds individually into multiple devices for large-scale analyses. The seeds may get contaminated or even destroyed during manual handling. To overcome this issue, we developed a hydrodynamic microfluidic trapping method to automatically load seeds into individual seed holding sites of the chip. Each trapping site was patterned like a funnel. The top opening of the funnel was large enough to allow a seed to come in, while the bottom opening was relatively smaller to prevent the seed from falling out of the funnel. Multiple seeds were infused into the main channel by flowing a liquid medium through the inlet of the device (Fig. 1a). A sucking pressure was applied through the outlet by withdrawing the fluid out of the device, forcing the seeds to flow against the lower wall of the main channel. As the seed flowed by a funnel, the fluid streamlines would carry the seed into the funnel. Since each funnel is designed to allow hosting of only one seed, other seeds have to flow over this funnel to the following ones, allowing for a single seed to be trapped.

To better understand the seed trapping mechanism and to study the influences of the seed and device geometries, and the infusion and withdrawal flow rates on the seed trapping, we conducted fluid dynamic simulations for the device by using finite element analysis (FEA) software COMSOL. A model was thus built for the simulation (Fig. 2a). The key structural and geometrical parameters include the widths of the top and bottom openings (W_t and W_b, respectively) and the depth of the funnel (L), the height or width of the main channel (H), the lengths of the semi-major and semi-minor axes of the seed (a and b, respectively), and the ratio of a to b or a/b. Because the present device was designed for phenotyping of *Arabidopsis* plants, based on the possible sizes and shapes of different types of *Arabidopsis* seeds, we set reasonable dimension ranges for the aforementioned parameters as follows: $1 \le a/b \le 2.25$, $0.3\ \text{mm} \le a \le 0.6\ \text{mm}$, $1 \le H \le 3\ \text{mm}$, $2a < W_t < 4a$, $W_b < 2b$, and $2a < L < 4a$.

All of the FEA simulations were conducted under a rotational equilibrium condition that a seed was assumed to move axially without rotation while moving in the main channel. Through extensive simulational trials, the rotational equilibrium of the seeds was achieved at an angle of about 30 degrees between the seed's semi-major axis and the longitudinal direction of the main channel. The criteria for successful seed trapping were that the volumetric centre of the seed should be located above a critical streamline (highlighted by the white lines in Fig. 2b–h) that starts at the input of the main channel and ends at the upper-right corner of the funnel.

We first studied how the pressure drop ΔP over a trapping site along the main channel impacted the seed trapping. Fig. 2b shows that when the volumetric centre of the seed was located above one-third the height or width of the main channel from the lower horizontal sidewall of the main channel, the seed would pass by rather than flowing into the funnel under a low $\Delta P = 0.5$ Pa. To simplify, all of the seeds in the following simulations were set to flow against the lower sidewall of the main channel. Fig. 2c indicates that regardless of the lateral distance x between the seed and the funnel, the seed could be trapped into the funnel as long as the seed was flowing against the sidewall under $\Delta P = 0.5$ Pa. But as ΔP gradually increased to 2 Pa (Fig. 2d), the critical streamline moved closer to the sidewall and overlapped the volumetric centre of the seed (see the first panel from the right in Fig. 2d). This indicates that by applying a higher ΔP, the seed would pass by the funnel.

Subsequently, the influence of the shape and size of a seed on the seed trapping was studied. The simulated results show that as the value of a/b increased from 1 to 2.25 while keeping $a = 400$ μm (Fig. 3e) or as the seed was scaled up in all dimensions while keeping $a/b = 2$ (Fig. 3f), the seed would be trapped under a low $\Delta P = 0.5$ Pa as long as the volumetric centre of the seed was located below the corresponding critical streamline.

In addition, the influence of the structure of the main channel and the funnel on the seed trapping was investigated. The simulated result shows that increasing the width of the top opening of the funnel caused the critical streamline to elevate, which, in turn, would make it easier to trap the seed (Fig. 2g). On the other hand, as the width of the main channel increased from 1 to 3 mm, the seed flowing along against the lower sidewall of the main channel would still be trapped (Fig. 2h).

It is worthwhile to point out that since dimensional variations among different types of *Arabidopsis* seeds are actually minor (at the size scale of several hundreds of micrometres), it should be relatively easy to tune the key structural parameters of the device to adapt to different seeds, without the need of establishing a new model for simulations.

Experimentally, in order for the seed to flow in the lower part of the main channel, a pulling pressure was applied at the outlet of the device (Fig. 1a and 2a). Thus, two syringe pumps were simultaneously used during seed trapping, one for infusion and the other for withdrawal of fluid. We experimentally studied how the infusion/withdrawal flow rates affected the trapping rate of *Arabidopsis* seeds. Here, the trapping rate refers to the success rate of trapping *one or two* seeds in a funnel. It is noted that trapping two seeds in a single funnel was possible as the sizes and shapes of the seeds (of even the same type) were not uniform. Fig. 3a demonstrates that (i) as the withdrawal flow rate increased from 0 to 20 $\mu L\ s^{-1}$, the trapping rate increased from 4.6 ± 2.9% to 97 ± 2.2%; (ii) the lower the infusion flow rate, the

easier the seed trapping, and thus, the higher the trapping rate, which followed the trend seen in Fig. 2h; and (iii) the trapping rate decreased gradually and then relatively abruptly with increasing the infusion flow rate from 5 to 75 μL s^{-1}. Fig. 3b shows the experimental results of how the width of the main channel affected the trapping rate. As W_t increased from 1.4 to 3 mm, the seeds flowing in the lower part of the main channel relatively reduced in quantity, and thus, the

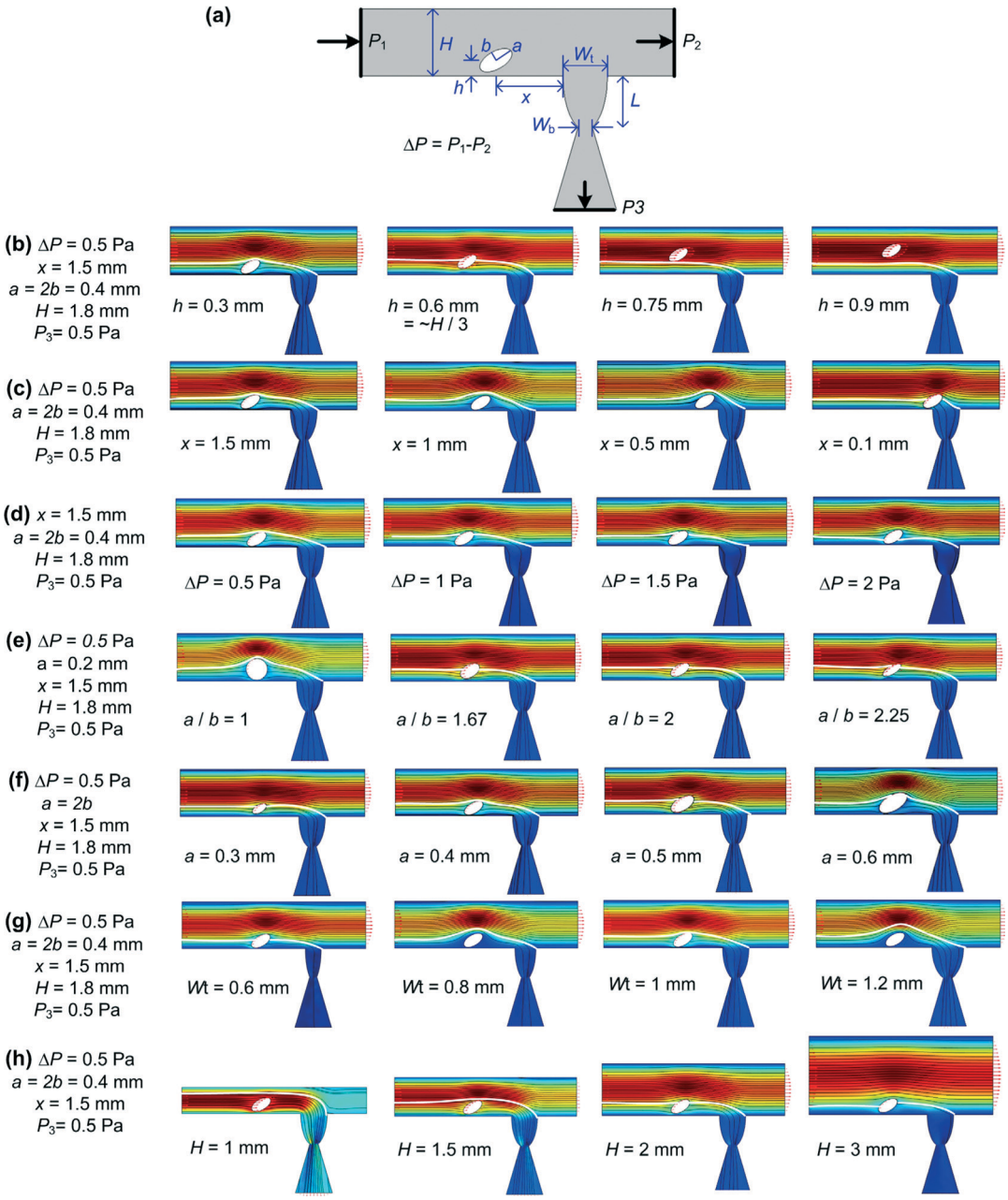

Fig. 2 (a) A FEA model for simulating fluid dynamics during hydrodynamic trapping of a seed into a funnel-like trapping site. (b) Distributions of fluid velocity when the seed is flowing at different distances from the lower sidewall of the main channel in the vertical direction. From left to right, h = 0.3, 0.6, 0.75, and 0.9 mm, respectively. (c) Distributions of fluid velocity when the seed is located at different distances from the upper left corner of the funnel in the longitudinal or horizontal direction. From left to right, x = 1.5, 1, 0.5, and 0.1 mm, respectively. (d) Distributions of fluid velocity under different pressure drops along the main channel over a single trapping site in the longitudinal direction. From left to right, $\Delta\Delta P$ = 0.5, 1, 1.5, and 2 Pa, respectively. (e) Influence of the shape of a seed on the distribution of fluid velocity. From left to right, a/b = 1, 1.67, 2, and 2.25, respectively, while a is fixed at 0.2 mm. (f) Influence of the size of a seed on the distribution of fluid velocity. From left to right, a = 0.3, 0.4, 0.5, and 0.6 mm, respectively, while a/b is fixed at 2. (g) Influence of the width of the top opening of the funnel on the distribution of fluid velocity. From left to right, W_t = 0.6, 0.8, 1 and 1.2 mm, respectively, while W_b is fixed at 0.3 mm. (h) Influence of the height or width of the main channel on the distribution of fluid velocity. From left to right, H = 1, 1.5, 2, and 3 mm, respectively. In (a)–(h), the colour scale represents the fluid velocity, where red indicates high and blue indicates low. The white lines added to the distribution profiles of fluid velocity represent the critical streamlines.

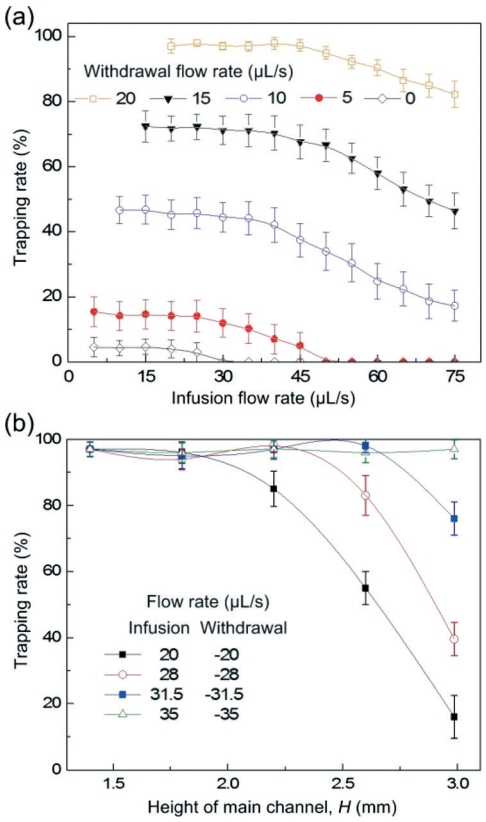

Fig. 3 (a) Experimental result of the seed trapping rate as a function of infusion flow rate for different withdrawal flow rates. *Arabidopsis* seeds used here has a/b = 1.88 ± 0.2. (b) Experimental result of the trapping rate as a function of the width of the main channel at different infusion and withdrawal flow rates. The trapping sites used here are shown in Fig. 2b. Each measurement is the mean ± standard deviation obtained from 10 measurements.

trapping rate was observed to decrease from 97 ± 2.2% to 16 ± 6.5% at the infusion flow rate of 20 μL s^{-1} and the withdrawal flow rate of −20 μL s^{-1}. It should be noted that by increasing the withdrawal flow rate, the trapping rate of the device having a wider channel could be increased to be nearly 100% as demonstrated in Fig. 3b.

Device fabrication

The microfluidic devices were fabricated using a conventional soft lithography technique.[37] Briefly, to make a master mould for the microchannels, a silicon wafer was first patterned with SU-8 photoresist (Microchem, MA, USA). Then, a high-resolution transparency film (10 160 dpi, Fineline Imaging, CO, USA) was used as a photomask in photolithography. A prepolymer mixture of polydimethylsiloxane or PDMS (Sylgard 184, Dow Corning, MI, USA) and its curing agent with a weight ratio of 10 : 1 was poured onto the master mould and then thermally cured on a hotplate at 90 °C for 1 hour. Subsequently, the hardened PDMS polymer was pealed from the mould and bonded to a microscope glass slide (75 mm × 50 mm × 0.9 mm) by using oxygen plasma treatment. Lastly, the inlet and outlet ports of the device were manually punched with a mechanical puncher.

It should be pointed out that the formation of the PDMS-based structures on a glass slide is not expected to modify *Arabidopsis* growth patterns. PDMS-glass microfluidic devices have been widely used in characterization of both cellular and multicellular organisms.[28,38,39] Moreover, *Arabidopsis* plants are routinely grown in glass flasks containing hydroponic growth media for biochemical and physiological studies. As discussed in Table 1, our results show that the growth stages for *Arabidopsis* plants grown in the fabricated devices were comparable to those grown in conventional Petri dish. This further demonstrates that materials used for the fabrication of the devices had little or even no influence on the growth patterns of *Arabidopsis* plants.

Culture media

Three different liquid culture media were prepared and used, including tap water, Murashige and Skoog (MS) medium, and standard medium.[40] All of the chemicals used were of analytical reagent grade. Deionized water was used throughout to prepare the three nutrient media. MS salts were purchased from Sigma-Aldrich, MO, USA. Culture media were sterilized in an autoclave at 15 psi at 121 °C for 30 min and stored at 4 °C in a refrigerator. They were loaded into the device using a 3 mL syringe (Becton Dickinson, NJ, USA) with a microbore tubing (Cole-Parmer, IL, USA) before the seeds were transferred into the device.

Preparation of *Arabidopsis* seeds

Wild-type (WT) *Arabidopsis thaliana* ecotype Columbia, the *immutans* mutant of *Arabidopsis*, and transgenic *Arabidopsis* seeds containing the *IM* promoter green fluorescent protein (GFP) reporter fusion construct were used in this study. GFP activity assays were performed using confocal laser scanning microscopy with seeds and seedlings grown within the device. The seeds were surface-sterilized by soaking in 70% ethanol (v/v) for 1 min, followed by 50% (v/v) Clorox and 0.02% (v/v) Triton for 15 min. They were then washed three times with autoclaved deionized (DI) water.

To trap and hold *Arabidopsis* seeds in the vertical device, the lower opening size of the seed holding site must be less than the small diameter of the oval shaped seed. But if the lower opening was made too small, the root growth of the seeds would be influenced due to the limited space. Therefore, *Arabidopsis* seeds were soaked in a Petri dish containing autoclaved DI water for 3–5 h and allowed to expand in size slightly prior to loading.

Trapping of *Arabidopsis* seeds

Before seed trapping, all channels in the device were filled with one particular culture medium of interest by using a syringe *via* a tubing connection. Care was taken to avoid introducing air bubbles into the channels. Subsequently, the soaked seeds were sucked manually from the soaking Petri dish up into a 500 μm inner diameter microbore tubing using a syringe. The tubing was then connected to the inlet

Table 1 Comparison of growth stages for WT *Arabidopsis* plants growing in a microfluidic device and Petri dish[a]

	Microfluidic device (days)			Plate (days)
Growth stage	Tap water	MS	Standard	Agar + MS[45]
Seed coat breakage	0.8 ± 0.2	1.2 ± 0.2	1.0 ± 0.2	ND
Radicle emergence	1.2 ± 0.2	1.7 ± 0.3	1.2 ± 0.2	1.3 ± 0.4
Length of primary root (0.6 mm)	2.2 ± 0.2	2.0 ± 0.2	2.2 ± 0.3	ND
Cotyledon & hypocotyl emergence	2.5 ± 0.2	2.2 ± 0.1	2.0 ± 0.2	2.5 ± 0.6
Cotyledons fully opened	3.0 ± 0.2	3.0 ± 0.1	3.0 ± 0.2	3.0 ± 0.5
2 rosette leaves	9.0 ± 0.3	8.0 ± 0.2	8.0 ± 0.3	7.3 ± 0.5

[a] Note: all data exclude days of stratification.

port of the device. After that, a syringe pump (KDS200, KD Scientific, MA, USA) was used to inject the seeds directly from the tubing into the device through the inlet port at an infusion flow rate of 20 μL s^{-1}. The other syringe pump (same model) applied a sucking pressure through the outlet of the device at a withdrawal flow rate of −20 μL s^{-1}, forcing the seeds to flow along the lower sidewall of the channel. It took 3–4 s to complete the seed trapping process.

Arabidopsis plant growth conditions

After the seeds were trapped in the seed holding sites, the device was stored at 4 °C in a refrigerator for 40–48 h to stratify the seeds. Subsequently, the device was placed vertically under a plant growth light source (fluorescent daylight). The light intensity was set to ~100 μE m^{-2} s^{-1}, and plants were grown at room temperature (21–22 °C). The environmental relative humidity was ~40%. For the top-closed device (Fig. 1a and b), growth media were changed in the device on a daily basis using a syringe pump. In the case that the main channel was opened, the fluid level in the device was controlled by slowly flowing growth media (2–3 μL h^{-1}) into the device using a syringe pump through the port where sucking force was applied during the seed trapping process (see Fig. 1b). The seeds germinated and the plants grew in the device, and their growth was monitored after exposure to light (or starting from the completion of stratification).

A microscope (MZ 205FA, Leica, Germany) with a video camera (QICAM, QImaging, Canada) was used to image plants growing in the device. The system was used to collect phenotypic data of interest, including seed phenotype (*e.g.*, germination), root phenotype (*e.g.*, length, diameter), shoot phenotype (*e.g.*, hypocotyl, cotyledon and leaf emergence and dimensions), and cell phenotype (*e.g.*, cell division and elongation). All data points reflect the average from five replicates performed on five chips, with each chip having 20–26 plants on a device. Error bars represent standard deviations.

Results and discussion

Hydrodynamic seed trapping

Fig. 4 shows the results of the hydrodynamic seed trapping method (also see video clip in ESI†). Almost all of the seed holding sites in the device held seeds. 70–80% of these sites had a *single* seed while the rest of the sites trapped more than one seed. This is because the *Arabidopsis* seeds were not uniform in size and multiple smaller seeds could be trapped into one holding site. We observed that after a seed fell into a trapping site, other seeds were not trapped. The percentage of the trapped seeds with respect to the total input seeds was 30–40%. The untrapped seeds were flowed out of the device.

Seed germination and plant growth

As a first step to optimize *Arabidopsis* growth within the device, we tested three different hydroponic media (tap water, MS medium and standard medium) previously used in conventional tissue culture methods. Fig. 5 shows time-lapse images for the development of *Arabidopsis* plants inside the devices containing the three different growth media. Plant growth and development, including root and shoot systems, were continuously monitored up to 11 days, and images were taken at regular intervals while the plants were growing

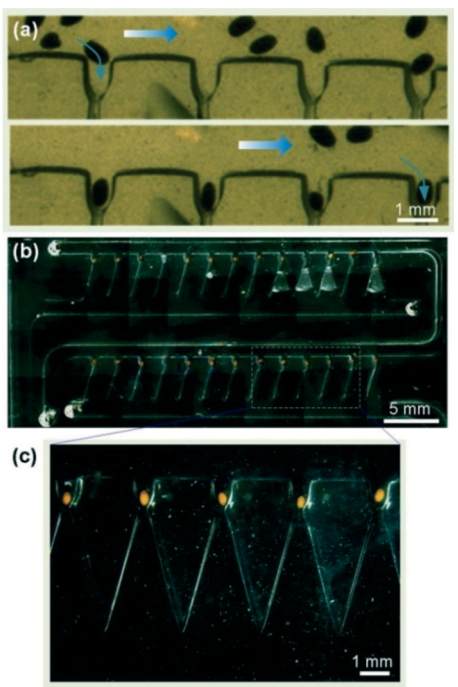

Fig. 4 (a) Hydrodynamic trapping of *Arabidopsis* seeds. (b) Microfluidic plant chip after seed trapping process. (c) Magnified image showing individual seeds trapped in seed holding sites.

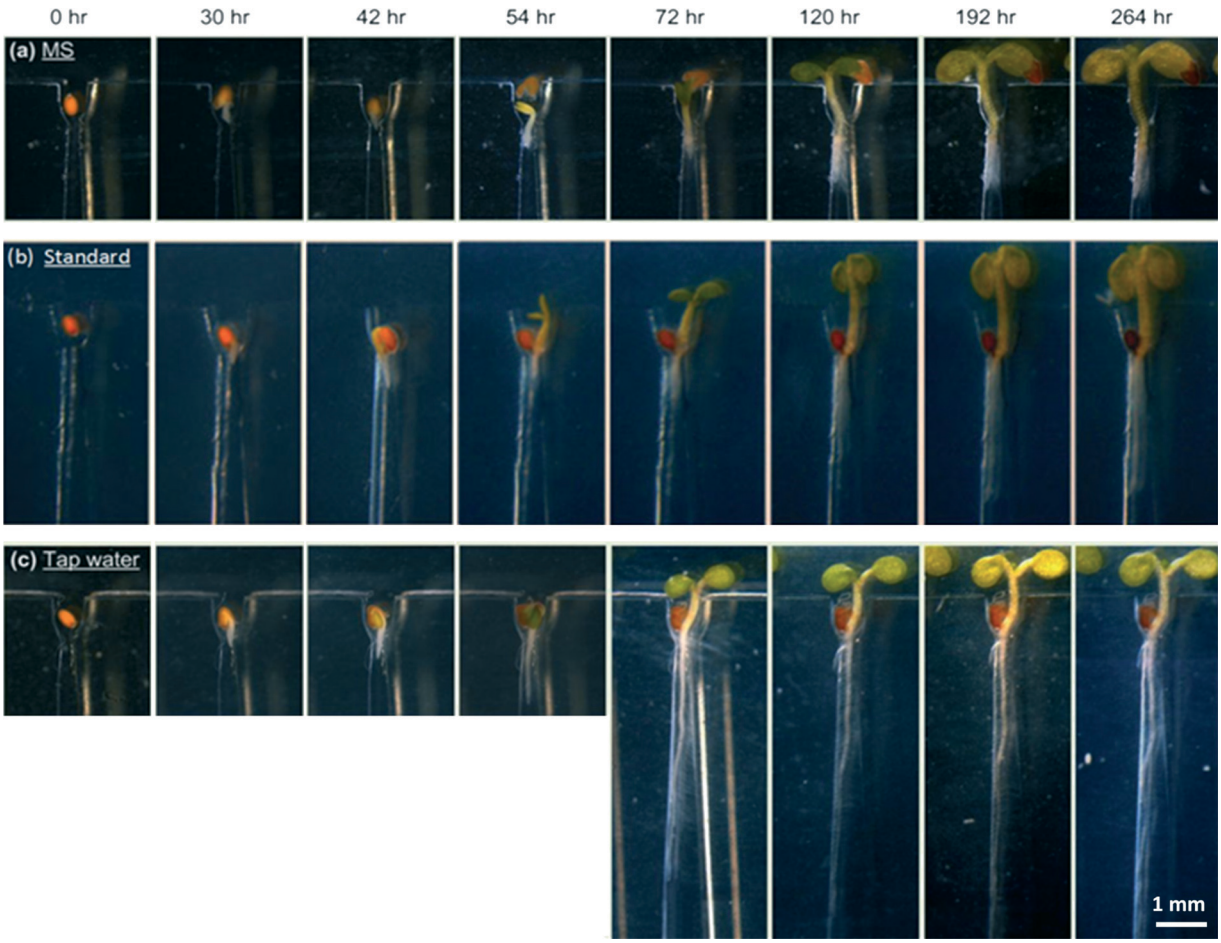

Fig. 5 Seed germination and growth of WT *Arabidopsis thaliana* plants in the vertical microfluidic device with (a) MS medium, (b) standard medium, and (c) tap water.

inside the device. Plants grown in all three media appeared to maintain all of the morphological and physiological traits of plants grown in potting soil and on a Petri plate.

Arabidopsis seeds generally follow a two-step germination process with rupture of the seed coat in 20–24 h and the emergence of the white radicle following endosperm rupture in 30–33 h.[41] As shown in Fig. 5, in-chip germination of *Arabidopsis* seeds was similarly comparable to the previously reported results with observation of a radicle after around 30 h in light in all growth media. It should be noted that due to different orientation of the seeds in the holding sites, the radicles of many seeds were not oriented initially downward. But as the roots grew longer, they tended to grow along a sidewall of the holding sites, and then, entered downward into the tapered growth region towards the bottom of the device. Quantitative analysis of root length as a function of growth time (Fig. 6a), where root length was measured as the distance from the root tip to the base of the hypocotyl, shows that the roots grew rapidly up to 5 days, but slowly thereafter. Furthermore, in agreement with previously reported literature,[41–45] the roots growing in tap water were observed to be longer and thinner with sparser root hairs while those growing in MS media and standard media were shorter and wider with a greater number of root hairs. As expected, the green cotyledons were observed to grow up towards the light and in opposite direction to the roots (Fig. 5). The emergence and growth of the hypocotyl and cotyledon of *Arabidopsis* plants growing within the device could be conveniently imaged and quantitatively analysed over 11 days without manual intervention. The growth of hypocotyl was similar for all plants in different growth media (Fig. 6b). However, the growth and size of the cotyledons were significantly influenced, with MS medium showing the greatest increase in the surface area (Fig. 6c). The time-frame for emergence of cotyledons was similar in all media with the two cotyledons emerging approximately 52–54 h after exposure to light, following which they grew rapidly for 11 days of plant growth.

To assess whether WT *Arabidopsis* growth and development within the microfluidic device were similar to *a priori* data, we compared our results with the plants germinated and grown on conventional tissue culture plates.[46] Table 1 shows that the timeline for many of the plant growth stages was highly comparable between the conventional plate method and the newly developed device. However, slight variations between these two methods were also observed. For example, the appearance of 2 rosette leaves is somewhat

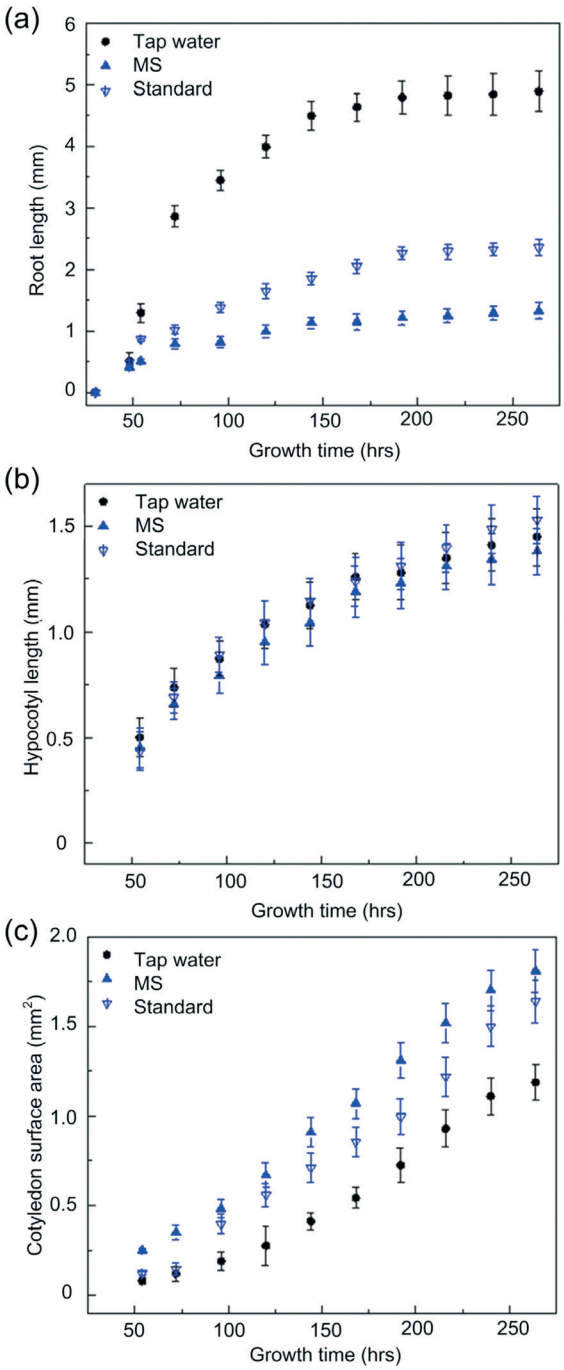

Fig. 6 Major phenotypic parameters of WT *Arabidopsis thaliana* plants as a function of growth time, including (a) root length, (b) hypocotyl length, and (c) cotyledon surface area. The data were obtained by using Matlab based on the images taken at different time points.

delayed (in hours) when compared to the Petri plate method. It should be noted that a Petri plate-based method generally uses gelling *agar* to prevent seeds from rolling, while plants in our device grew in hydroponic media and the seeds were held by microstructures. Thus, these discrepancies may be caused by differences in geometric structure of growth chambers (channels *vs.* plates) or the surrounding physical environment of seeds (liquid *vs.* agar gel). These discrepancies are negligibly small and would not interfere with high-throughput plant phenotyping as long as phenotypic comparisons between different genotypes and plant organs can be simultaneously observed.

Phenotyping of *Arabidopsis* mutants

We used a well-characterized carotenoid-deficient mutant, the *immutans* (*im*) mutant of *Arabidopsis*,[47,48] as an example to demonstrate general utility of the present device for phenotyping *Arabidopsis* plants, at the whole organismal as well as at the cellular level. The *immutans* mutant of *Arabidopsis* has green-white leaves due to a mutation in the nuclear recessive gene, *IMMUTANS* (*IM*). The *im* seeds have been previously shown to germinate similar to WT *Arabidopsis* under various light conditions. Our results show that *im* seeds germinate and grow under normal light conditions also within the device (Fig. 7). However, we further show that seed germination and radicle protrusion occur much earlier (~12 h) in *im* when compared to WT *Arabidopsis* (~20 h). Although the exact reason for this phenomenon is not known, it is clear that the new device enables more in-depth exploration and quantitation of the seed germination process in a real-time manner.

Depending on the light intensity, germinated seedlings of *im* give rise to green, green-white and/or white cotyledons and leaves. An increase in light intensity increases white sector formation whereas low light conditions result in all-green plants. Consistent with previous reports, the cotyledons of *im* growing in-chip under normal light conditions are white and/or green with the green being somewhat lighter than WT. Seedlings with white cotyledons do not give rise to true leaves and are not viable after 11 days of growth in the hydroponic medium, whereas green coloured seedlings grow true leaves after ~194 h of growth (Fig. 7). Under our growth conditions, *immutans* root and hypocotyl lengths are somewhat similar to WT (Fig. 8a and b). But the growth of the cotyledons slows down significantly after ~8 days of growth (Fig. 8c). This is in agreement with the slower growth phenotype of *im* plants *versus* WT *Arabidopsis*.

To obtain a more detailed cellular description of the *Arabidopsis im* phenotype, we applied confocal laser scanning microscopy (CLSM) and fluorescence stereomicroscopy (Leica M205FA), and performed *in vivo im* gene expression analyses using transgenic *IM*-GFP seeds/plants. The *IM* promoter β-glucuronidase (GUS) activity assays have previously shown that *IM* is expressed in all shoot and root tissues throughout the development of *Arabidopsis* plants.[48] Similarly, in this study, we show an *IM* promoter-GFP activity in 1 day, 5 day and 7 day old seedlings, with green fluorescence observed in all tissues including root, hypocotyl, and cotyledons (Fig. 9 and 10). The 5 and 7 day old low resolution images were obtained with the fluorescence stereomicroscope equipped with a GFP filter set to image whole seedlings. This expression pattern was also maintained in developing leaves and roots, with increased expression observed in the root tips, as seen in the images in Fig. 10. Moreover, *im* expression

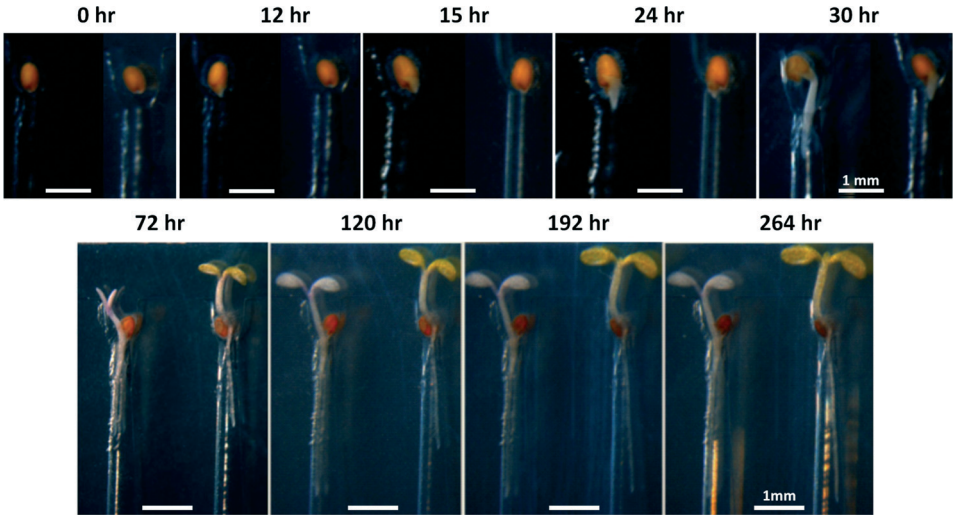

Fig. 7 Time course study of growth and development of WT *Arabidopsis* and *immutans* plants growing in a standard medium in the vertical microfluidic device.

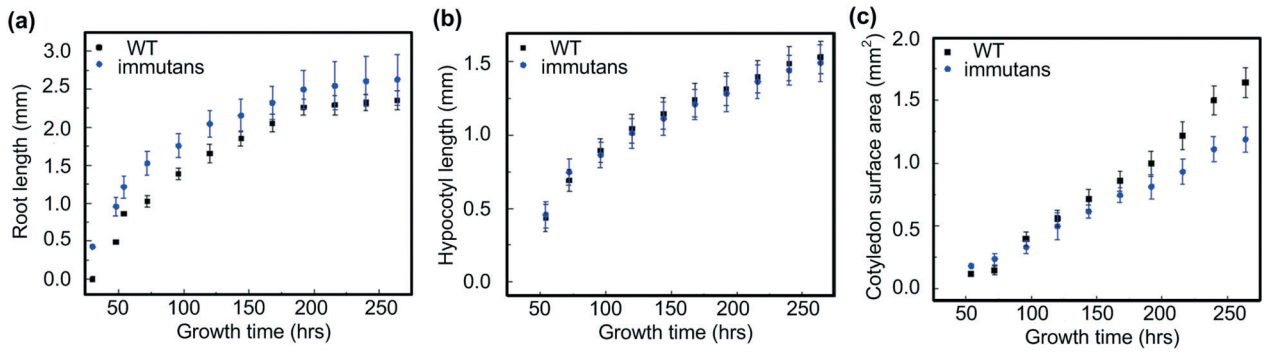

Fig. 8 Major phenotypic parameters of WT *Arabidopsis* and *immutans* mutant as a function of growth time, including (a) root length, (b) hypocotyl length, and (c) cotyledon surface area.

was found to be restricted to the chloroplasts within individual cells in green tissues (Fig. 10e), which is consistent with the function of *IM* in plants. However, our results suggest that *im* is also expressed very early in the seed germination process. This is illustrated by the presence of green fluorescence first in regions around the embryo, even prior to seed coat breakage and radicle protrusion. Subsequently, the GFP fluorescence extends into the embryo and then into the protruding radicle as the seed germinates (Fig. 11a–c). These results could not be observed previously with GUS activity assays, perhaps due to the fact that the GFP reporter, unlike the GUS reporter, allows nondestructive monitoring of cellular and sub-cellular activities without the need for sample preparation or the uptake of exogenous substrate. No GFP fluorescence was observed in non-transgenic WT control seeds and seedlings (data not shown).

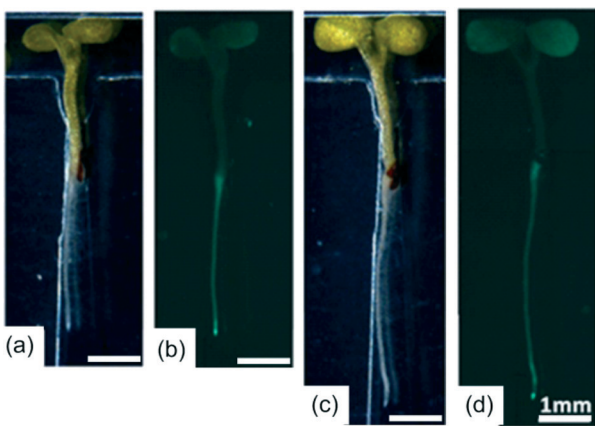

Fig. 9 Growth of *IM* GFP plants in the vertical microfluidic device. Optical images (a, c) and fluorescence images (b, d) of 5 day and 7 day old seedlings, respectively.

Plant–pathogen interactions

As another example of the utility of the present device for plant phenotyping, we show results from a study of plant–pathogen interactions. Specifically, we demonstrate early interactions of *Phytophthora sojae* zoospores with wild-type *Arabidopsis* plants on the vertical microfluidic device. Fungal and oomycete pathogens such as *P. sojae* cause many destructive

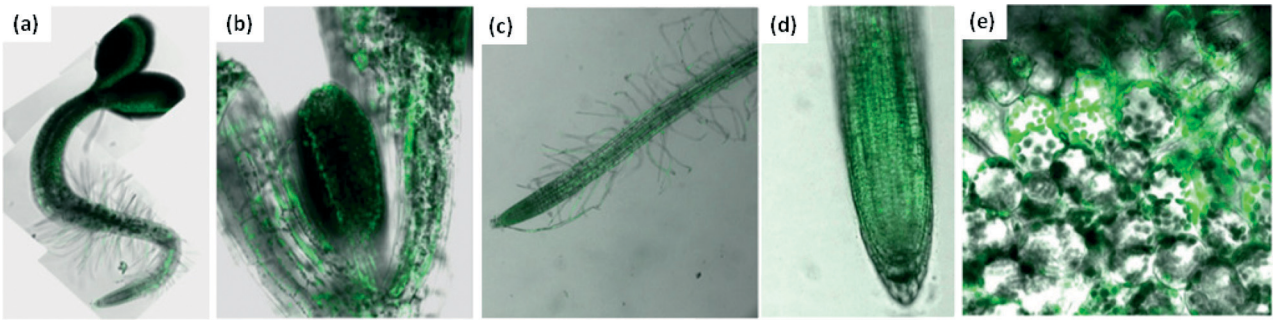

Fig. 10 Confocal laser scanning microscopy images for *IM GFP* seedlings growing in the device. (a) 1 day old seedlings at a magnification of 10×. (b) 5 day old leaves at 20×. (c) 5 day old root at 10×. (d) 5 day old root tip at 40×. (e) 5 day old cotyledons at 80×.

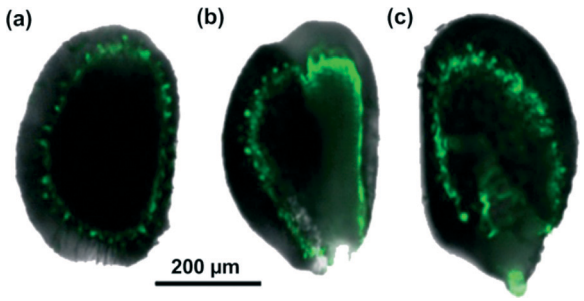

Fig. 11 Time course study of the seed germination process of *IM* GFP seeds growing in the vertical device. (a) 0 h, (b) 12 h, and (c) 18 h, after 2 day stratification.

diseases of plants and genetic approaches pose difficulty for observing early phenotypic interactions between pathogens and plant roots and shoots.[49,50] *P. sojae* zoospores were flowed into the vertical device with tap water at 24 h after the *Arabidopsis* seeds were trapped into the seed holding sites. The motile zoospores swam randomly until the root radicles emerged. High resolution images show that the zoospores accumulated down at the root tip and root hairs 5–10 h after their adhesion to the device (Fig. 12a), and then, they started invading the root and the shoot systems. At ~50 h, multiple dark brown spots were observed on the root, which are the symptoms of apoptosis and cell death (Fig. 12b). Several dark brown spots were also observed on the emerging cotyledons and hypocotyl at later stages of infection.

These spots were observed all the way toward the cotyledon, particularly at the intersection between the hypocotyl and root, indicating severe invasion and growth of zoospores inside these organs (Fig. 12c and d).

Top-opened device for phenotyping *Arabidopsis* plants over a longer period of growth

In general, growth and development of WT *Arabidopsis* did not appear to be affected during its 11 day growth in the microfluidic device; however, the device presented above used a closed-top design, which in turn limited the space of the channels above the seed holding site for shoot growth. Hence, the shoot phenotype could be monitored only through the stage of emergence of two rosette leaves on the plants. To accommodate developmental stages beyond the 2-leaf stage, we further created a top-open device in which the main channel above the seed holding site is open to air. This allowed for observing and recording cotyledon and leaf phenotypes over a longer period of growth. Specifically, after *Arabidopsis* seeds were trapped, the top part of the channel above the seed holding sites was manually cut off by a razor blade. The level of growth medium in the device was adjusted by slowly flowing a growth medium into the device as described earlier. Fig. 13 shows *Arabidopsis* plants grown for a longer period of 15 days in the top-opened device in a standard medium. The standard medium allowed similar and measurable growth of both shoot and root regions when compared to the other two media. Similar to observations made with the closed device, we observed radicle emergence at ~32 h, and the hypocotyl and cotyledon emergence at ~54 h. The two early rosette leaves were observed at ~192 h, and then, more leaves emerged in the following days. The leaves were growing upward outside the channel while the roots were still elongating inside the channel. At the end of

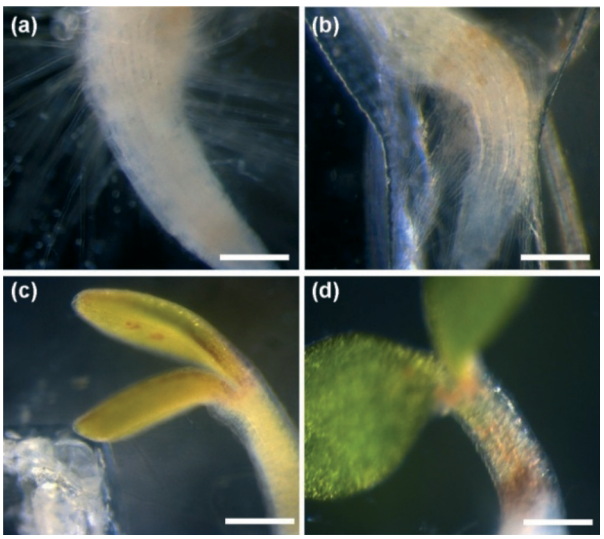

Fig. 12 (a) Formation of clusters of *P. sojae* zoospores on the root and root hairs of *Arabidopsis* plant, observed at 31 h. Dark brown spots on the root (b), cotyledon (c), and hypocotyl (d), observed at 50 h, 124 h, and 192 h, respectively. Scale bars are 100 μm.

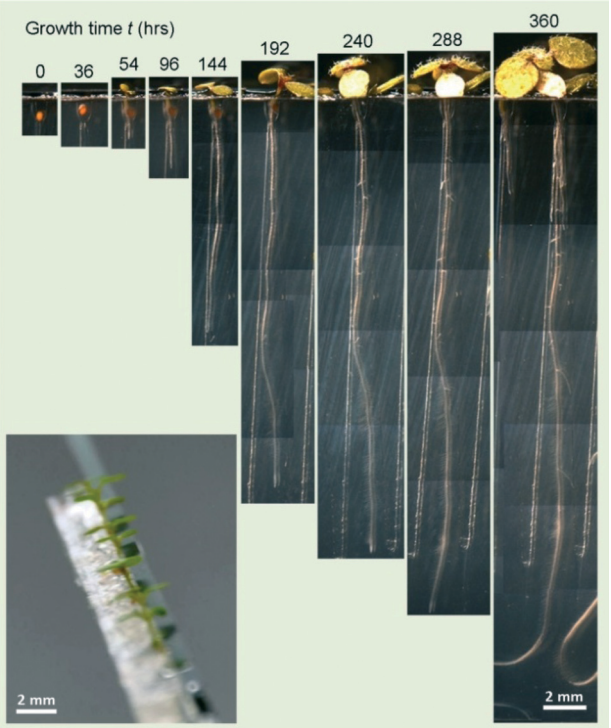

Fig. 13 Growth of a WT *Arabidopsis thaliana* plant over 15 days in the top-open vertical microfluidic device. The inset in the bottom-left corner shows cotyledons and leaves growing out of the vertical device.

15 days, we observed 5 rosette leaves. This is consistent with previous reports of plants growing on MS agar plates where 5 rosette leaves developed at 14.7 ± 1.8 days (excluding 3 days of stratification).[46] Thus, by simply opening up the main channel above the seed holding sites, the issue of limited growth space inside the device could be largely eliminated, which would make it possible to observe and record plant phenotypes through later growth stages, thus further expanding the utility of the device for plant phenotyping.

Conclusion

Systematic characterization of plant phenotypes remains a major challenge due to their large genome sizes and tens of thousands of genes which respond differentially to various external and internal stimuli. Because of this inherent complexity, analyzing plant phenotypes on a large and multi-scale level with sufficient throughput, resolution and precision has been difficult and expensive. Previous work has addressed this challenge to some extent, but these studies were mainly focused on phenotyping of roots.[32–36] In this paper, we demonstrate the development of a new microfluidic device that is easy and cost-effective to use, and also enables seamless monitoring of both root and shoot phenotypes. We have provided a few examples and applications of the prototype device in this study. However, the device design can be flexibly changed to further enhance its application in the plant phenomics area. For example, with a top-open device (Fig. 13), plants can be grown over longer periods of time, allowing for different and multiple types of *Arabidopsis* genotypes to be simultaneously characterized at the physiological, biochemical and molecular level, and at various stages of growth. In fact, the vertical device was able to sustain plant growth for over 4 weeks (data not shown).

Further research and development remain to be done to realize an ultimate screening platform for high-throughput plant phenotyping. Other microfluidic and microsystem techniques can be developed and integrated into this present microfluidic device. Through microfluidic tuning, flexible control over chemical concentration and composition in each growth channel can provide a large number of different nutrimental, chemical and biological environments for the plants growing in the microfluidic device. Different means of generating concentration gradients have been demonstrated,[51–54] such as using universal concentration generator and on-chip dilution approach. Also, to control plant growth temperature, a simple thin-film resistive heater and temperature sensor can be integrated on the plant chip. These types of modifications will further expand the utility of the present device as multiple plants can be analysed under different environmental conditions in a single experiment. Furthermore, by employing an automated robotic imaging system, it is possible to take a large number of images for different plant growth regions in the devices. Therefore, we believe that the present vertical microfluidic plant chip technology can contribute towards establishing a powerful experimental framework for high-throughput and precise plant phenotyping, and it will create a paradigm-shift in the plant phenomics area.

Acknowledgements

This work is supported by the National Science Foundation and by the Plant Sciences Institute at Iowa State University through the Interdisciplinary Innovative Research Grants Program. The authors thank Dr. Wei Hong (Aerospace Engineering, Iowa State) for providing help in fluid dynamics FEA simulations, Dr. Madan Bhattacharya (Agronomy, Iowa State) for providing zoospores, Dr. Steve Rodermel (Genetics, Development, and Cell Biology, Iowa State) for the transgenic *Arabidopsis* seeds used in CLSM, Dr. Santosh Pandey (Electrical and Computer Engineering, Iowa State) for helpful discussions, and Margie Carter for help in confocal laser scanning microscopy, and all other group members in the Laboratory for MEMS and Lab-Chips for technical assistance.

Notes and references

1 T. Thorsen, S. J. Maerkl and S. R. Quake, *Science*, 2002, **298**, 580–584.
2 J. Melin and S. R. Quake, *Annu. Rev. Biophys. Biomol. Struct.*, 2007, **36**, 213–231.
3 S. R. Quake and A. Scherer, *Science*, 2000, **290**, 1536–1540.
4 M. A. Unger, H. P. Chou, T. Thorsen, A. Scherer and S. R. Quake, *Science*, 2000, **288**, 113–116.

5 C. Bolle, A. Schneider and D. Leister, *Curr. Genomics*, 2011, **12**, 1–14.
6 T. Kuromori, T. Wada, A. Kamiya, M. Yuguchi, T. Yokouchi, Y. Imura, H. Takabe, T. Sakurai, K. Akiyama, T. Hirayama, K. Okada and K. Shinozaki, *Plant J.*, 2006, **47**, 640–651.
7 T. Kuromori, S. Takahashi, Y. Kondou, K. Shonozaki and M. Matsui, *Plant Cell Physiol.*, 2009, **50**, 1215–1231.
8 D. Houle, D. R. Govindaraju and S. Omholt, *Nat. Rev. Genet.*, 2010, **11**, 855–866.
9 R. T. Furbank and M. Tester, *Trends Plant Sci.*, 2011, **16**, 635–644.
10 P. K. Gupta, S. Rustgi and R. R. Mir, *Heredity*, 2008, **101**, 5–18.
11 J. D. Hoheise, *Nat. Rev. Genet.*, 2006, **7**, 200–210.
12 P. Liu, N. Koizuka, T. M. Homrichhausen, J. R. Hewitt, R. C. Martin and H. Nonogaki, *Plant J.*, 2005, **41**, 936–944.
13 D. C. Boyes, A. M. Zayed, R. Ascenzi, A. J. MacCaskill, N. E. Hoffman, K. R. Davis and J. Gorlach, *Plant Cell*, 2001, **13**, 1499–1510.
14 A. Sessions, E. Burke, G. Presting, G. Aux, J. McElver, D. Patton, B. Dietrich, P. Ho, J. Bacwaden, C. Ko, J. D. Clarke, D. Cotton, D. Bullis, J. Snell, T. Miguel, D. Hutchison, B. Kimmerly, T. Mitzel, F. Katagiri, J. Glazebrook, M. Law and S. A. Goff, *Plant Cell*, 2002, **14**, 2985–2994.
15 M. R. Ponc1, P. Robles and J. L. Micol, *Mol. Gen. Genet.*, 1999, **261**, 408–415.
16 J. M. Alonso, A. N. Stepanova, T. J. Leisse, C. J. Kim, H. M. Chen, P. Shinn, D. K. Stevenson, J. Zimmerman, P. Barajas, R. Cheuk, C. Gadrinab, C. Heller, A. Jeske, E. Koesema, C. C. Meyers, H. Parker, L. Prednis, Y. Ansari, N. Choy, H. Deen, M. Geralt, N. Hazari, E. Hom, M. Karnes, C. Mulholland, R. Ndubaku, I. Schmidt, P. Guzman, L. Aguilar-Henonin, M. Schmid, D. Weigel, D. E. Carter, T. Marchand, E. Risseeuw, D. Brogden, A. Zeko, W. L. Crosby, C. C. Berry and J. R. Ecker, *Science*, 2003, **301**, 653–657.
17 Q. Dong, S. D. Schlueter and V. Brendel, *Nucleic Acids Res.*, 2004, **32**(suppl. 1), D354–D359.
18 R. Subramanian, E. P. Spalding and N. J. Ferrier, *Mach. Vision Appl.*, 2013, **24**, 619–636.
19 P. Zimmermann, M. Hirsch-Hoffmann, L. Hennig and W. Gruissem, *Plant Physiol.*, 2004, **136**, 2621–2632.
20 J. K. C. Rose, S. Bashir, J. J. Giovannoni, M. M. Jahn and R. S. Saravanan, *Plant J.*, 2004, **39**, 715–733.
21 M. M. Bushey and J. W. Jorgenson, *Anal. Chem.*, 1990, **62**, 161–167.
22 V. Zabrouskov, L. Giacomelli, K. J. van Wijk and F. W. McLafferty, *Mol. Cell. Proteomics*, 2003, **2**, 1253–60.
23 L. W. Sumner, P. Mendes and R. A. Dixon, *Phytochemistry*, 2003, **62**, 817–36.
24 A. S. Iyer-Pascuzzi, O. Symonova, Y. Mileyko, Y. Hao, H. Belcher, J. Harer, J. S. Weitz and P. N. Benfey, *Plant Physiol.*, 2010, **152**, 1148–1157.
25 E. M. Lucchetta, J. H. Lee, L. A. Fu, N. H. Patel and R. F. Ismagilov, *Nature*, 2005, **434**, 1134–1138.
26 G. M. Whitesides, *Nature*, 2006, **442**, 368–373.
27 N. Chronis, M. Zimmer and C. I. Bargmann, *Nat. Methods*, 2007, **4**, 727–731.
28 K. Chung, M. M. Crane and H. Lu, *Nat. Methods*, 2008, **5**, 637–643.
29 P. Liu, R. J. Martin and L. Dong, *Lab Chip*, 2013, **13**, 650–661.
30 P. Liu, D. Mao, R. J. Martin and L. Dong, *Lab Chip*, 2012, **12**, 3458–3466.
31 C. G. Agudelo, A. S. Nezhad, M. Ghanbari, M. Naghavi, M. Packirisamy and A. Geitmann, *Plant J.*, 2013, **73**, 1057–1068.
32 G. Grossmann, W. Guo, D. W. Ehrhardt, W. B. Frommer, R. V. Sit, S. R. Quake and M. Meier, *Plant Cell*, 2011, **23**, 4234–4240.
33 H. Jiang, Y. Jiao, M. R. Maneesha and L. Dong, *J. Nanosci. Nanotechnol.*, 2012, **12**, 6333–6339.
34 M. Meier, E. M. Lucchetta and R. F. Ismagilov, *Lab Chip*, 2010, **10**, 2147–2153.
35 W. Busch, T. M. Brad, M. Bradley, D. L. Mace, R. W. Twigg, J. Jung, I. Pruteanu-Malinici, S. J. Kennedy, G. K. Fricke, R. L. Clark, U. Ohler and P. N. Benfey, *Nat. Methods*, 2012, **9**, 1101–1106.
36 A. Parashar and S. Pandey, *Appl. Phys. Lett.*, 2011, **98**, 263703.
37 D. B. Weibel, W. R. DiLuzio and G. M. Whitesides, *Nat. Rev. Microbiol.*, 2007, **5**, 209–218.
38 A. S. Reyhani, J. Kaplinsky, E. Burgin, M. Novakova, A. J. deMello, R. H. Templer, P. Parker, M. A. Neil, O Ces, P. French, K. R. Willison and D. Klug, *Lab Chip*, 2011, **11**, 1256–1261.
39 D. D. Carlo, L. Y. Wu and L. P. Lee, *Lab Chip*, 2006, **6**, 1445–1449.
40 P. Berthomieu, G. Conéjéro, A. Nublat, W. J. Brackenbury, C. Lambert, C. Savio, N. Uozumi, S. Oiki, K. Yamada, F. Cellier, F. Gosti, T. Simonneau, P. A. Essah, M. Tester, A. A. Véry, H. Sentenac and F. Casse, *EMBO J.*, 2003, **22**, 2004–2014.
41 P. P. Liu, N. Koizuka, T. M. Homrichhausen, J. R. Hewitt, R. C. Martin and H. Nonogaki, *Plant J.*, 2005, **41**, 936–944.
42 T. Ingestad and G. I. Agren, *Ecol. Appl.*, 1991, **1**, 168–174.
43 H. Zhang, A. J. Jennings and B. G. Forde, *J. Exp. Bot.*, 2000, **51**, 51–59.
44 H. Zhang and B. G. Forde, *Science*, 1998, **279**, 407–409.
45 H. Zhang, A. Jennings, P. W. Barlow and B. G. Forde, *Proc. Natl. Acad. Sci. U. S. A.*, 1999, **96**, 6529–6534.
46 D. C. Boyes, A. M. Zayed and R. Ascenzi, *Plant Cell*, 2001, **13**, 1499–1510.
47 C. M. Wetzel, C. Z. Jiang, L. J. Meehan, D. F. Voytas and S. R. Rodermel, *Plant J.*, 1994, **6**, 161–175.
48 M. Aluru, H. Bae, D. Wu and S. Rodermel, *Plant Physiol.*, 2001, **127**, 67–77.
49 W. Grunewald, G. van Noorden, G. van Isterdael, T. Beeckman, G. Gheysen and U. Mathesius, *Plant Cell*, 2009, **21**, 2553–2562.
50 N. Wuyts, G. Lognay, R. Swennen and D. De Waele, *J. Exp. Biol.*, 2006, **57**, 2825–2835.

51 C. Hao and M. J. Christian, *Appl. Phys. Lett.*, 2004, **84**, 2193–2195.
52 N. L. Jeon, S. K. W. Dertinger, D. T. Chiu, I. S. Choi, A. D. Stroock and G. M. Whitesides, *Langmuir*, 2000, **16**, 8311–8316.
53 X. Jiang, Q. Xu, S. K. W Dertinger, A. D. Stroock, T. M. Fu and G. M. Whitesides, *Anal. Chem.*, 2005, **77**, 2338–2347.
54 D. Irimia, D. D. A. Geba and M. Toner, *Anal. Chem.*, 2006, **78**, 3472–3477.